HAL
open science

A parameter to probe microdroplet dynamics and crystal nucleation

R. Grossier, Victoria Tishkova, R. Morin, S. Veesler

To cite this version:

R. Grossier, Victoria Tishkova, R. Morin, S. Veesler. A parameter to probe microdroplet dynamics and crystal nucleation. AIP Advances, 2018, 8 (7), pp.075324. 10.1063/1.5034443 . hal-01744090v2

HAL Id: hal-01744090

https://hal.science/hal-01744090v2

Submitted on 24 Aug 2018

HAL is a multi-disciplinary open access archive for the deposit and dissemination of scientific research documents, whether they are published or not. The documents may come from teaching and research institutions in France or abroad, or from public or private research centers.

L'archive ouverte pluridisciplinaire **HAL**, est destinée au dépôt et à la diffusion de documents scientifiques de niveau recherche, publiés ou non, émanant des établissements d'enseignement et de recherche français ou étrangers, des laboratoires publics ou privés.

July 2018 Volume 8 Number 7

AIP Advances

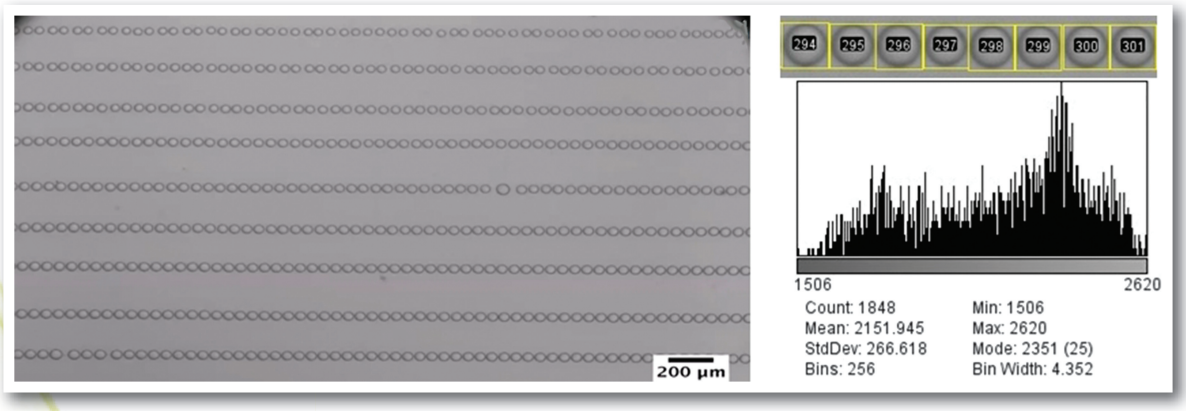

A parameter to probe microdroplet dynamics and crystal nucleation

DOI: 10.1063/1.5034443

advances.aip.org

AIP ADVANCES **8**, 075324 (2018)

A parameter to probe microdroplet dynamics and crystal nucleation

R. Grossier,[a] V. Tishkova, R. Morin, and S. Veesler[a]
Centre Interdisciplinaire de Nanoscience de Marseille, CINaM - CNRS, Aix-Marseille Université Campus de Luminy, Case 913, F-13288 Marseille Cedex 09, France

(Received 11 April 2018; accepted 28 June 2018; published online 24 July 2018)

We present a simple and efficient digital-image processing method to simultaneously monitor the contraction of a statistically relevant number of microdroplets of the same size and the nucleation of single salt crystals inside. Each individual microdroplet image is reduced to a scalar, standard deviation σ of the grey-level of pixels inside a region of interest containing the microdroplet image, and overall microdroplet dynamics is monitored using standard-deviation time-evolution plots. It is shown that this approach makes it possible to measure the nucleation time and also that microdroplets interact via water diffusion dynamics. This effect actually decreases the nucleation rate, contrary to previous findings. This "σ approach" can be compared to recording the order parameter in phase transition, which makes it ideal for studying dynamics of systems where images are the primary outputs. © *2018 Author(s). All article content, except where otherwise noted, is licensed under a Creative Commons Attribution (CC BY) license (http://creativecommons.org/licenses/by/4.0/).*
https://doi.org/10.1063/1.5034443

Microdroplets (μDs) are a versatile experimental tool for visualising, characterising or measuring physicochemical properties.[1] They can be studied for themselves to reveal how sensitive to local environment their dynamics are (evaporation, dissolution or contraction)[2–5] or to make phenomena occur at specific locations[6–8] or to perform multiple experiments where statistics are of importance.[9] However, studying the dynamics of a statistically significant number of μDs requires the analysis of a huge amount of data. Here we probe μD dynamics using 2D ensemble of roughly 10^3 μDs of salted water immersed in an oil film and subjected to water evaporation, leading to nucleation of single crystals of salt. Under these conditions, weakly contrasted images are acquired every second for roughly 10^3 seconds. The million images thus yielded clearly exceed our aims: to monitor μD dynamics and crystal nucleation time. What we show here is that the state of a μD at a given time t can simply and efficiently be described by a scalar σ(t), a quantity easily extracted from an image of this μD at time t. This scalar is the standard deviation of the grey-level of pixels inside a region of interest (ROI) containing the μD image. This approach makes it possible to measure the nucleation time and also reveals that μDs interact via water diffusion. Importantly, this effect is shown to decrease the nucleation rate, contrary to previous findings.[10] Although closer to an information model than a physical model, this "σ approach" is similar to recording the order parameter in phase transition. This makes it ideal for studying the dynamics of systems where images are the primary outputs.

Our work can be seen as an extension of the work of Schäfle et al.,[11] who presented a simple method to quantify the temporal evolution of an ordered array of μDs leading to a superlattice through cooperative effects between μDs. They measured the mean pixel histogram intensity ratio for carefully selected μD pairs at different superlattice sites during evaporation. They observed that under certain conditions the μDs do not evaporate independently but cooperatively, by matter exchange through the gas phase. However, the method has several limitations. First, ordered arrays of μDs needs to be prepared using a patterned surface. Second, μDs needs to be examined in pairs to compare their

[a]Phone: +336 6292 2866, Fax: +334 9141 8916, grossier@cinam.univ-mrs.fr; veesler@cinam.univ-mrs.fr

 © Author(s) 2018

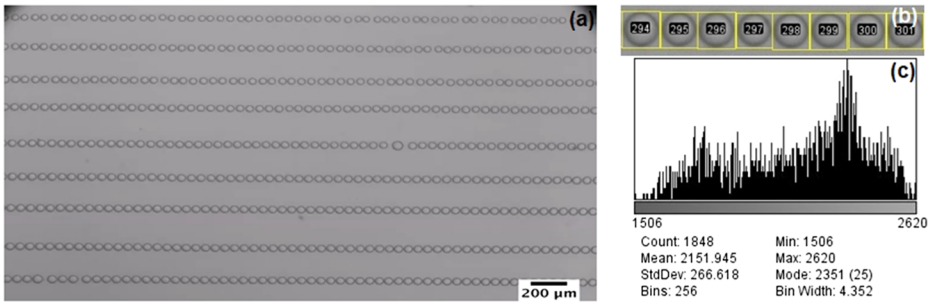

FIG. 1. **Array1** (a) immediately after generation, bottom line (line 9) is the most recently generated, 527 µDs with initial droplet radius of 25.1µm ±0.8 (for line 9), with a volume of 60.7pL assuming a contact angle of 130°,[17] (b) µDs with the ROI of a magnified area of (a) (line 6 from the top) at t=133s after the generation of **Array 1** (see video S1 (supplementary material) for a movie of the microdroplet dynamics) and (c) grey level histogram for the ROI of µD 294 at t=270s.

relative evaporation rate. Third, intensity ratios can only be used to indicate a cooperative process when evaporation rates are clearly different. Another experimental approach was proposed by Bonn et al.[12] to demonstrate the interaction between a collection of small monodisperse droplets. They used a precision balance to monitor the mass of the evaporating system. While both approaches[11,12] are elegant, they do not provide information on individual µD contraction. Our approach overcomes many of these limitations.

Here, arrays of sessile µDs are generated by a microinjector on an oil-covered 18mm-diameter glass coverslip treated so as to obtain a surface preventing µDs from spreading and coalescing (Fig. S1), as described previously[13] (additional details available in supplementary material). Two µD arrays are presented (Figs. 1 and S2), both prepared under the same conditions except for relative humidity % in room atmosphere (RH) above DMS oil and initial µD radius (R) (see supplementary material).

Both µD generation and subsequent contraction are observed under a transmission optical microscope. We stop imaging when contraction of each µD has reached completion: all the water in the µD has diffused through oil and there is a NaCl crystal at each µD position (Fig. S3 of the supplementary material). The first image just after µD generation (Fig. 1) is processed using FIJI software (Image J, NIH, USA). After thresholding and binarisation procedures, we use the "Analyze Particles" plugin to individually detect each µD position and size. A rectangular ROI is then assigned to each µD (Figs. 1(b) and S4). From this ROI, comprising a single µD and its immediate vicinity, we extract the histogram of pixel grey-levels (Fig. 1(c)). We focus on its standard deviation σ, a measure of the homogeneity of pixel grey-levels.[14] As each individual µD and its immediate vicinity, on each image, is reduced to a single number (σ), µD time evolution can be monitored throughout associated ROI standard deviation time evolution (ROI, σ, t), as reported for a single µD in Fig. 2(a). Each (ROI, σ, t)-plot is then processed with home-made PYTHON codes (www.python.org) to extract characteristic points (the code is available on request).

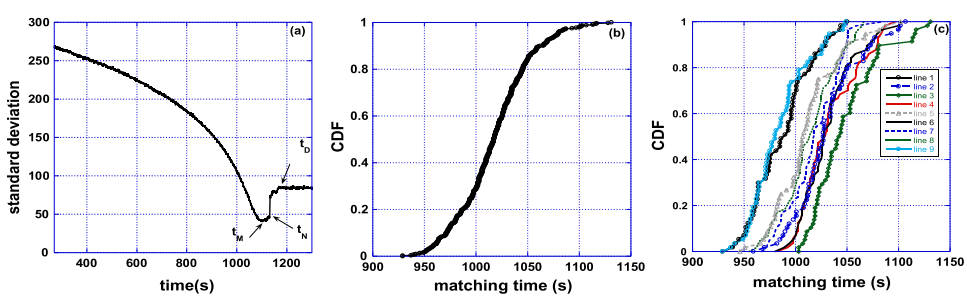

FIG. 2. (a) (ROI, σ, t)-plot of µD#294 of **Array 1** (Fig. S4a of the supplementary material). t_M-CDF of **Array 1** (b) for the 527 µDs, and (c) line-by-line, line 1 to line 9 from top to bottom of Fig. 1.

The μD contraction process leading to crystal nucleation was previously described in Ref. 15, and is recalled here (Fig. S3 and video S1 of the supplementary material). Throughout the contraction process, water is leaving the μD, thus increasing NaCl concentration. This increases the μD refractive index, which leads to two characteristic stages. First, as the μD starting refractive index is lower than the DMS index, the μD refractive index will gradually increase until it matches the DMS refractive index exactly. At this matching time (t_M) the μD optically disappears and NaCl concentration can be estimated from an extrapolated relation between concentration and refractive index (tables 71 D-252).[16] Second, as the contraction process proceeds, the μD refractive index will exceed the DMS refractive index: the μD gradually reappears until sudden nucleation occurs at nucleation time (t_N). Then a single crystal rapidly grows, before the μD dries completely at drying time (t_D).

Taking a single μD (assumed spherical cap, due to their small size compared to the capillary length, 2.7mm for a water droplet), with a starting concentration of 0.025 of the NaCl saturation value, the volume has to be divided by 40 before saturation concentration is reached. In terms of measurement dynamics, μD diameter explores one order of magnitude (50.2 μm at generation, 14.9 μm at saturation and in micrometer range at nucleation), volume explores two orders of magnitude (60.7 pL to <1pL), and the resulting crystal is in the micrometre range. Such spatial dynamics make it difficult to apply measurement techniques where spatial resolution is required: image resolution decreases with the number of μDs simultaneously observed. Considering magnification alone (1.3μm per pixel here), while some uncertainty on starting diameter is acceptable (2.6μm for a 50μm diameter μD, i.e $\Delta D/D$=5% error), this no longer applies when μDs reach 14.9μm diameter. At this point, $\Delta D/D$=17.4%, which, translated into volume, corresponds to an uncertainty of $\Delta V/V$ = 52.2%. Moreover, the size of the resulting crystal is similar to the resolution. Added to this spatial resolution issue, the vanishing refractive index difference (Δn) between continuous phase (here DMS oil) and dispersed phase (μDs) does not simplify measurements: edge contrast will fade and disappear during part of the contraction process. At a minimum, these limitations prevent the usual optical techniques from determining t_M where the μD is both small and optically invisible, and under certain conditions also prevent determination of nucleation time t_N.

By reducing μD and its vicinity (the ROI) to a single scalar like σ, we identify the μD signal as any departure from system noise. It is in fact a differential point probe measurement approach similar to signal-to-noise ratio measurement (defined as σ^2/μ, with μ = mean of the signal), except that we only focus on standard deviation of the full grey-level distribution of pixels inside the ROI. At the refractive index matching time, t_M, σ is minimum: this is the standard deviation of the noise of our system. Anywhere else (before and after t_M), the grey-level distribution of pixels contained in the ROI, and the associated σ, results from the μD contraction process via the interplay between illumination path, μD geometry (diameter, contact angle, height) and difference in refractive index, Δn, with surrounding media. Three populations of pixels and their associated grey-level distribution can be distinguished, each contributing to the signal σ emerging from the ROI. (1) Those in the vicinity of the μD, fixed by the system noise. (2) The brightness decay zone, extending from μD edge toward centre, fixed by Δn and the μD geometry, both determined by Brewster and total internal reflexion angles relative to illumination path. (3)- The central μD area, where light absorption occurs along the direct light path. The balance of pixel grey-level distributions associated with these populations gives rise, throughout μD contraction, to the measured signal and its evolution: σ-curves (Fig. 2(a)).

The variation of σ in the vicinity of t_M is related to Δn: it decreases before t_M, and increases afterwards. This makes t_M a global minimum on the σ-curve, easy to find numerically. In a previous paper we observed a constant μD contraction rate for pure water and in different salts,[17] thus from t_M and NaCl concentration in the μD at that time we can easily deduce the linear contraction rate of each μD in the array, which is proportional to the reverse of t_M.

At t_N, the smooth evolution of σ throughout the contraction process is hindered by the nucleation and fast growth of a crystal inside the μD. This clear and sudden jump of σ to higher values is easy to determine with simple thresholding procedures. Then, the nucleated crystal will grow until the μD completely dries, t_D. Note that precise determination of t_D requires more sophisticated algorithms than this simple minimum determination and thresholding, and will not be addressed here.

The information obtained here on each individual μD from (ROI, σ, t)-plots is sparse compared to the usual approaches (side-views systems)[17–19] where, with the help of highly resolved images,

geometrical μD parameters (diameter, contact diameter, contact angle, height) are monitored. However, our approach overcomes the acknowledged limitations to the study of collective contraction effects,[12,18,20] such as the low number of droplets in the patterns (limiting statistical validity) and their large size (possible convection). For instance, for the 527 μDs in **Array 1**, we plot in Fig. 2(b) the t_M cumulative distribution frequency (CDF). Despite the monodisperse μD starting sizes,[13] they do not contract at the same rate, which might appear to be due solely to their different local pinning conditions. However, when μD position in the array is taken into account in plotting line-by-line t_M-CDF (Fig. 2(c)), the main reason for such a wides contraction rate distribution is revealed: collective effects, i.e. neighbour-dependent contraction rates. This results from the instantaneous water concentration field and subsequent gradients a μD will experience, fixed both by itself and by neighbouring μDs. Comparing the general trend from one μD line to another (Fig. 2(c)), we see high similarity in the shape of their respective CDFs. This results from a spatial scale common to all lines: the μD-to-μD first-neighbour distance within a line is uniform throughout the array (at generation time). Only local pinning due to impurity will modify this uniformity. The shift in t_M-CDF mean values for each line comes from another spatial scale, line-to-line distance, by far larger and less uniform than μD-to-μD first-neighbour distance within a line. External array lines (1 and 9) only have a single neighbouring line (respectively 2 and 8), which explains why they statistically contract faster. For the inner lines, the position of t_M mean values is a function of its distance from the two neighbouring lines, and line 5 is the most representative of this behaviour: it is the fastest of the inner lines, being the farthest from neighbouring lines.

Interestingly, there is good superimposition of both outer lines (1 and 9) CDFs: despite being generated at different times and different spatial locations on the substrate, they still present the same CDF. This validates the μD generation method and confirms the homogeneity of the PMMA substrate: while local pinning still occurs, we observe enough μDs to make it appear as noise on the CDF shape shown by both lines. To resume, the difference between two CDFs comes from differences both in μD diameters and local pinning, but the statistical approach allows us to identify a common CDF. The plots of **Array 2** t_M-CDF show the same trends (Figs. S5a and S5b of the supplementary material).

Moreover, our approach makes it possible to measure nucleation induction times of each μD in the array. Nucleation induction time is the time over which a system can withstand supersaturation, constant or increasing,[21] before nucleation occurs. In the context of nucleation studies, accurate nucleation induction time measurement has always been difficult to achieve. The main experimental difficulty comes from the stochastic aspect of the nucleation process: we do not know where, when and how many such events occur. Moreover, the size of the critical nucleus is in the nanometre range, requiring either measurement systems addressing the nanoscale (in-situ electron microscopy,[22,23] AFM,[24,25] laser confocal microscopy[26]), or highly resolved current measurement (using an external localized DC electric field with a nanoelectrode[27]). Because of these difficulties, such small-scale experiments are not performed routinely and their quantitative relevance is still to be confirmed. Consequently, most experiments address the microscale, for instance using turbidity measurements.[28] However, this is quite a large system compared to the supposed size of critical clusters. The price to pay is that assumptions on the nucleation mechanism have to be made in order to model both growth of individual nucleated clusters and their possible interactions (like Ostwald ripening) until the crystal can be detected.[29,30] Here, we present experiments in which the statistical approach is guaranteed through the large number of identical crystallisers (μDs) that can be monitored simultaneously. All μDs will lead to nucleation of only one crystal[31] and because of the fast growth rate (greater than $200 \mu m s^{-1}$[27]), the time required for the newly formed nuclei to grow to a detectable size is negligible with regard to the induction time.[32] Thus, these experiments allow us to measure real nucleation induction times without needing to make assumptions on the nucleation mechanism.

In the (ROI, σ, t)-plots, nucleation of a crystal inside the μD is seen through a sudden and large increase in σ (Fig. 2(a)). In Fig. 3(a), we plot the line-by-line CDF of t_N for the 527 microdroplets of **Array 1**. To take into account each μD individual contraction rate[17] which is proportional to the reverse of t_M, we normalise t_N relative to this rate: t_N is divided by t_M. The line-by-line CDF of normalised nucleation times is shown in Fig. 3(b), and across lines we observe a narrow and similar distribution of the measured normalised induction times. Such reproducibility in measurements already represents a step forward in experiments addressing nucleation mechanisms.

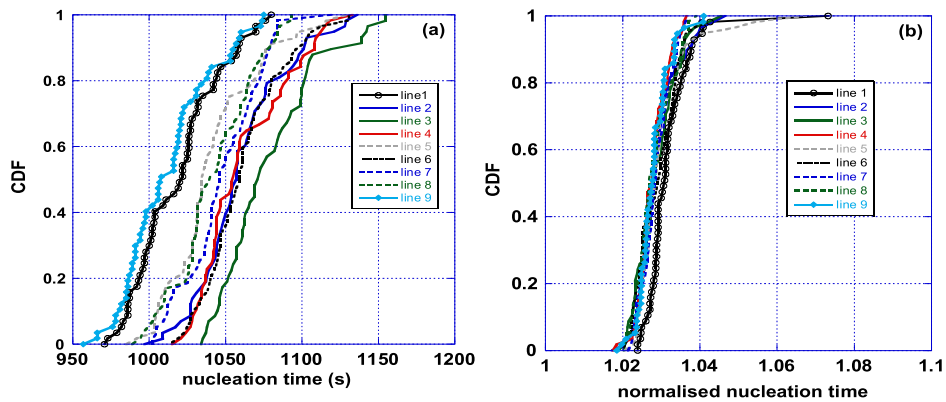

FIG. 3. (a) Line-by-line CDF of t_N: for the 527 μDs of **Array 1**, and (b) vs normalised nucleation time line-by-line.

μD-contraction can be represented as the sum of two contributions: a vertical water flux toward oil interface with atmosphere, and lateral water fluxes from μD to μD, both responsible for the collective effect. Any change in the experimental conditions (R, D, h, RH) will affect this balance, as demonstrated by **Array 2**. In practice, for **Array 1** μD-contraction, every (ROI, σ, t)-plot presents the same characteristic behaviour: a minimum is reached at t_M and σ values increase until there is a sudden jump corresponding to crystal nucleation (hereafter these curves are called type 1). For **Array 2** μD-contraction (Fig. S6 and video S2 (supplementary material) for a movie of the microdroplet dynamics) and t_N-CDF curve (Fig. S5c of the supplementary material), evolution of μDs seems similar to **Array 1** μDs. However, a closer look at **Array 2** (ROI, σ, t)-plots shows that some μDs present (ROI, σ, t)-plots with additional features compared to type 1 σ-curve characteristics (Figs. 4 and S7). For two neighbouring (Fig. 4) μDs, there is a temporal correlation between crystal nucleation in μD#641 (showing type 1 σ-curve) and a sudden drop in the σ-curve for μD#640. After this drop, σ reaches a minimum value and then increases again, until there is a sudden jump corresponding to crystal nucleation. σ-curves presenting such a correlated oscillation with nucleation in a neighbouring μD will hereafter be called type 2. The advantage of using (ROI, σ, t)-plots is clear here: both **Array 1** and **Array 2** would be mistakenly considered equivalent without this tool.

Collective effects influence μD contraction rates via the instantaneous water concentration field[11,12,18,20, and this work]. Moreover, a temporal correlation is observed between two neighbouring

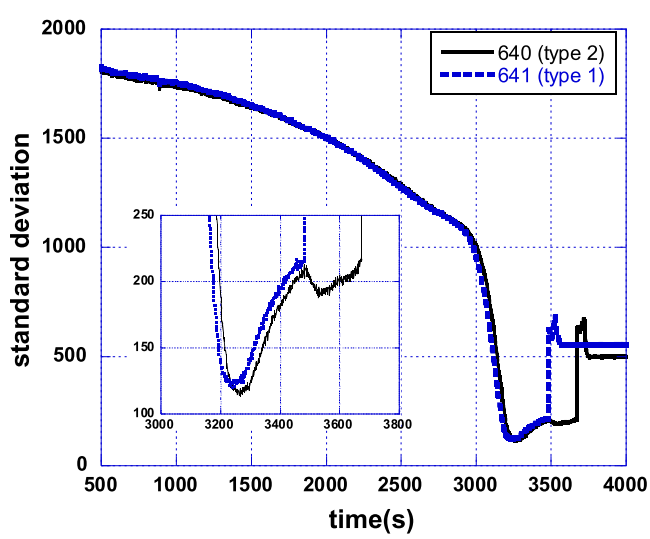

FIG. 4. Time evolution of standard deviation of neighbouring μDs 640 and 641 of line 8 of **Array 2**. Insert is a zoom in the nucleation zone.

μDs due to nucleation in one μD. When a crystal nucleates in a μD (μD#641, Fig. 4) its rapid growth abruptly decreases the Na^+ and Cl^- concentrations in the droplet. This suddenly increases the chemical potential of water inside the μD (toward the chemical potential of pure water). As a result, there is a sudden increase in water flux from this μD toward its surrounding μDs when they are close enough (μD#640, Fig. 4). These μDs without crystals will grow and thereby decrease their solute concentration. As a consequence, both their Δn from surrounding oil and their σ will drop to lower values, as shown by oscillations present on type 2 σ-curves.

Now that we have identified this type 2 behaviour, it is clear that it needs to be taken into account when crystallisation is studied. The hypothesis that each μD can be considered independent of the others can now be tested before assuming that a true statistical view of nucleation is obtained. While collective effects during μD contraction can easily be corrected through normalisation relative to t_M (Fig. 3(b)), this is not the case for collective effects due to crystal nucleation: the independence required for statistical induction time measurements of contracting μDs is not respected. Although we expected to find interactions, the mechanism shown here is the opposite of those suggested.[10] In fact, the nucleation of a crystal in a μD does not trigger but delays nucleation in neighbouring μDs. Moreover, CDF shape is not significantly different regardless of whether nucleation-mediated interactions occur (Fig. S6c of the supplementary material) or not (Fig. 3(a)). (ROI, σ, t)-plots appear to be a useful tool both to determine μD independence and to provide data of good quality for nucleation studies.

The method presented in this paper allows us to simultaneously monitor the contraction of a statistically relevant number of μDs of the same size. The full time-sequence of images is processed to characterise μD dynamics. Every individual μD image is reduced to a scalar standard deviation (σ), and μD-contraction is monitored using standard-deviation time-evolution plots.

It is shown that this approach not only makes it possible to measure nucleation time but also that μDs interact via water diffusion. It is also shown that this effect decreases the nucleation rate, contrary to previous findings. Our "σ approach" can be compared to recording an order parameter in phase transition. This makes it ideal for studying the dynamics of systems where images are the primary outputs.

See supplementary material for microdroplet generation, time sequences of microdroplet dynamics of **Array 1 and 2**, CDF of characteristic times of **Array 2** and time evolution of standard deviation of neighbouring μDs 622 to 641 of line 8 of **Array 2**. Video S1 and S2 for movies of the microdroplet dynamics of **Array 1** and **2** respectively.

The authors would like to thank Marion Pellen and Marin Jourdan. We thank Marjorie Sweetko for English revision.

[1] S. Lee and J. Wiener, Journal of Chemical Education **88**(2), 151 (2010).
[2] M. He, C. Sun, and D. T. Chiu, Analytical Chemistry **76**(5), 1222 (2004).
[3] D. Brutin, B. Sobac, B. Loquet, and J. Sampol, Journal of Fluid Mechanics **667**, 85 (2011).
[4] R. D. Deegan, O. Bakajin, T. F. Dupont, G. Huber, S. R. Nagel, and T. A. Witten, Nature **389**, 827 (1997).
[5] V. Dugas, J. Broutin, and E. Souteyrand, Langmuir **21**(20), 9130 (2005).
[6] K. T. Rodolfa, A. Bruckbauer, D. Zhou, A. I. Schevchuk, Y. E. Korchev, and D. Klenerman, Nano Letters **6**(2), 252 (2006).
[7] F. De Angelis, F. Gentile, F. Mecarini, G. Das, M. Moretti, P. Candeloro, M. L. Coluccio, G. Cojoc, A. Accardo, C. Liberale, R. P. Zaccaria, G. Perozziello, L. Tirinato, A. Toma, G. Cuda, R. Cingolani, and E. Di Fabrizio, Nat. Photon. **5**(11), 682 (2011).
[8] K. K. B. Hon, L. Li, and I. M. Hutchings, CIRP Annals - Manufacturing Technology **57**(2), 601 (2008).
[9] P. Laval, A. Crombez, and J.-B. Salmon, Langmuir **25**(3), 1836 (2009).
[10] A. I. Toldy, A. Z. M. Badruddoza, L. Zheng, T. A. Hatton, R. Gunawan, R. Rajagopalan, and S. A. Khan, Crystal Growth & Design **12**(8), 3977 (2012).
[11] C. Schäfle, C. Bechinger, B. Rinn, C. David, and P. Leiderer, Physical Review Letters **83**(25), 5302 (1999).
[12] O. Carrier, N. Shahidzadeh-Bonn, R. Zargar, M. Aytouna, M. Habibi, J. Eggers, and D. Bonn, Journal of Fluid Mechanics **798**, 774 (2016).
[13] R. Grossier, Z. Hammadi, R. Morin, A. Magnaldo, and S. Veesler, Applied Physics Letters **98**(9), 091916 (2011).
[14] V. Kumar and P. Gupta, International Journal of Emerging Technology and Advanced Engineering **2**(8), 56 (2012).
[15] R. Grossier, A. Magnaldo, and S. Veesler, J. Crystal Growth **312**, 487 (2010).
[16] *Handbook of Chemistry and Physics* (CRC Press, Cleveland, 1975-1976).
[17] I. Rodríguez-Ruiz, Z. Hammadi, R. Grossier, J. Gómez-Morales, and S. Veesler, Langmuir **29**, 12628 (2013).
[18] A. J. D. Shaikeea and S. Basu, Langmuir **32**(5), 1309 (2016).
[19] C. Bourges-Monnier and M. E. R. Shanahan, Langmuir **11**(7), 2820 (1995).

[20] G. Laghezza, E. Dietrich, J. M. Yeomans, R. Ledesma-Aguilar, E. S. Kooij, H. J. W. Zandvliet, and D. Lohse, Soft Matter **12**(26), 5787 (2016).
[21] B. Peters, Journal of Crystal Growth **317**(1), 79 (2011).
[22] B.-S. Lee, G. W. Burr, R. M. Shelby, S. Raoux, C. T. Rettner, S. N. Bogle, K. Darmawikarta, S. G. Bishop, and J. R. Abelson, Science **326**(5955), 980 (2009).
[23] J. Baumgartner, A. Dey, P. H. H. Bomans, C. Le Coadou, P. Fratzl, N. A. J. M. Sommerdijk, and D. Faivre, Nat. Mater. **12**(4), 310 (2013).
[24] S. T. Yau and P. G. Vekilov, Nature **406**, 494 (2000).
[25] M. Sleutel, J. Lutsko, A. E. S. Van Driessche, M. A. Durán-Olivencia, and D. Maes, Nature Communications **5**, 5598 (2014).
[26] M. Sleutel and A. E. S. Van Driessche, Proceedings of the National Academy of Sciences **111**(5), E546 (2014).
[27] Z. Hammadi, R. Grossier, S. Zhang, A. Ikni, N. Candoni, R. Morin, and S. Veesler, Faraday Discussions **179**, 489 (2015).
[28] S. A. Kulkarni, S. S. Kadam, H. Meekes, A. I. Stankiewicz, and J. H. ter Horst, Crystal Growth & Design **13**(6), 2435 (2013).
[29] D. Kashchiev, D. Verdoes, and G. M. Van Rosmalen, J. Crystal Growth **110**, 373 (1991).
[30] G. M. Maggioni and M. Mazzotti, Crystal Growth & Design **17**(7), 3625 (2017).
[31] R. Grossier and S. Veesler, Cryst. Growth Des. **9**(4), 1917 (2009).
[32] R. Grossier, Z. Hammadi, R. Morin, and S. Veesler, Physical Review Letters **107**(2), 025504 (2011).